Magnetism and superconductivity in single-crystal $ErNi_2B_2C$

B. K. Cho, P. C. Canfield, L. L. Miller, and D. C. Johnston
Ames Laboratory and Department of Physics and Astronomy, Iowa State University, Ames, Iowa 50011

W. P. Beyermann and A. Yatskar
Department of Physics, University of California, Riverside, California 92521
(Received 15 March 1995)

The resistivity $\rho_{ab}(T)$ and anisotropic magnetization $M(T)$ of $ErNi_2B_2C$ crystals were measured as a function of applied magnetic field (**H**) from 2 to 300 K to study the magnetic and superconducting properties with **H** parallel and perpendicular to the c axis (**H**$\|$**c** and **H**$\perp$**c**). Low-temperature specific-heat measurements for $H=0$ show a lambda-shaped anomaly associated with antiferromagnetic (AF) ordering at $T_N=(5.85\pm0.15)$ K. The $\rho_{ab}(T)$ and $M(T)$ data show a superconducting transition at $T_c=10.5$ K, long-range AF ordering at $T_N=6.0$ K, and coexistence of superconductivity and antiferromagnetism below T_N. From the $\rho_{ab}(T)$ and $M(T)$ data, the T_N was found to be independent of H up to $H=20$ kG for **H**$\|$**c**, whereas for **H**$\perp$**c** T_N decreased as $\sim H^2$ from 6.0 K at $H=0$ to $T_N=3.2$ K at $H=18$ kG. The $M(T)$ data show a change in the easy axis direction from **H**$\|$**c** above 150 to **H**$\perp$**c** below 150 K. This change in anisotropy is associated with the anomalously small magnitude of the crystalline electric field B_2^0 term. The superconducting upper critical magnetic fields $H_{c2}(T)$ for **H**$\|$**c** and **H**$\perp$**c**, determined from $M(T)$ and $\rho_{ab}(H,T)$ data, show anomalies for both field orientations near T_N. However, the local minimum of $H_{c2}(T)$ near T_N, seen previously for both **H**$\perp$**c** and **H**$\|$**c** in a $HoNi_2B_2C$ crystal, was found only for **H**$\|$**c** in $ErNi_2B_2C$. This anisotropy in $H_{c2}(T)$ is likely a result of the anisotropy of the Er sublattice magnetization, specifically the anisotropy of $T_N(H)$. The depth of the local minimum in H_{c2} for **H**$\|$**c** for $ErNi_2B_2C$ near T_N is comparable to the one for $HoNi_2B_2C$ at 5 K.

I. INTRODUCTION

The interplay of superconductivity and magnetism has been an interesting topic in solid-state physics since the 1950's for experimentalists and theorists alike. The discovery of RMo_6S_6,[1] RMo_6Se_6,[2] and RRh_4B_4 (Ref. 3) (R = rare earth) compounds accelerated the research and led to much valuable information on the interrelationship of long-range magnetic order and superconductivity. Most of the pure superconducting compounds, however, showed magnetic transitions at temperatures below the liquid-helium temperature range (≤ 1 K). The discovery of the RNi_2B_2C (Refs. 4 and 5) (R = rare earth plus Sc, Y, and Th) compounds has rejuvenated the field, particularly since superconducting transition temperatures ($T_c \approx 8-17$ K) are relatively high and long-range antiferromagnetic (AF) ordering of the compounds containing magnetic rare-earth R ions is seen at temperatures ($T_N \approx 1.5-20$ K) more readily attained. The RNi_2B_2C compounds have a $ThCr_2Si_2$-type crystal structure with additional carbon atoms in each R layer. This structure consists of two-dimensional Ni_2B_2 layers connected by C atoms, forming cages for the R atoms.[6] Electronic band-structure calculations performed on $LuNi_2B_2C$ (Ref. 7) show that the Fermi energy coincides with the peak of a predominantly Ni $3d$ band density of states. They also suggest that despite their layered structure, these borocarbide compounds are electronically three dimensional and are more similar to conventional intermetallic superconductors than to the cuprate high-T_c superconductors.[7]

Large single crystals of RNi_2B_2C compounds grown in Ames Laboratory have made it possible to investigate the anisotropies of these compounds, which are potentially important because of their two-dimensional structural[6] and magnetic aspects.[8] The anisotropy in the magnetic-field-(H) dependent superconducting properties was studied in YNi_2B_2C (Ref. 9) and $TmNi_2B_2C$ (Ref. 10) crystals by analyzing the magnetization M data. These studies indicated that $H_{c2}(T)$ was isotropic for YNi_2B_2C and that $H_{c2}(T)$ became quite anisotropic in $TmNi_2B_2C$ for 2 K $< T <$ 6 K. The magnetic properties in the normal state, as well as in the superconducting state, of the rare-earth sublattice in a $HoNi_2B_2C$ ($T_c=8$ K) crystal were also studied in detail through magnetization measurements.[8] Neutron-scattering measurements have been widely performed to investigate the nature of the magnetic ordering. They found that $DyNi_2B_2C$ exhibits a commensurate AF ordering at $T_N=10.3$ K.[11] For $HoNi_2B_2C$, a transversely polarized spiral magnetic state was found in the superconducting state with an onset of 6 K followed by a commensurate AF ordering on further cooling to below 5 K.[12,13] For $ErNi_2B_2C$, and Er^{+3} magnetic moments order below 6 K in a transversely polarized planar sinusoidal structure.[14,15] In the case of $HoNi_2B_2C$ the influence of the AF ordering of the Ho^{+3} sublattice on superconductivity was found to be remarkable,[8,16] reviving interesting questions on magnetic pair breaking and stimulating other work. In this respect $ErNi_2B_2C$ should be studied very carefully in conjunction with the other RNi_2B_2C compounds. To this end, this paper presents a detailed study of the anisotropic magne-

0163-1829/95/52(5)/3684(12)/$06.00

tization and magnetoresistivity of $ErNi_2B_2C$. The data show anisotropies in the normal state as well as superconducting state for $\mathbf{H}\|\mathbf{c}$ and $\mathbf{H}\perp\mathbf{c}$. The observed anisotropies are compared with those of single crystal YNi_2B_2C, $TmNi_2B_2C$, and $HoNi_2B_2C$.[8–10]

II. EXPERIMENTAL DETAILS

Crystals of $ErNi_2B_2C$ were grown by an unusual high-temperature flux method using Ni_2B as a solvent. Ni_2B was chosen as a flux for several reasons. First, it has a melting point ($\approx$1100 °C) that is well below the decomposition temperature of $ErNi_2B_2C$ (> 1500 °C). Second, it introduces no new elements to the quaternary melt and therefore reduces the possibility of impurity phases. Third, based on studies of annealed polycrystalline samples[5] it seemed clear that, at least over a limited dilution range, RNi_2B_2C grew out of Ni_2B during arc melting and subsequent annealing.

The growth of large crystals was optimized by using the following steps. $ErNi_2B_2C$ is first prepared in polycrystalline form by arc melting a mixture of Er (Ames Lab: 99.99%), Ni (99.99%), B (99.5%), and C (99.99%) under argon gas on a water-cooled copper hearth. An excess of 5 wt. % B over that required for stoichiometry was added to the stoichiometric mixture to compensate the loss of mass during arc melting. The polycrystalline button, wrapped with Ta foil, is sealed in a quartz tube under a partial pressure of Ar and then annealed at 1050 °C overnight to encourage the further formation of the $ErNi_2B_2C$ phase. The powder x-ray-diffraction pattern of such an annealed sample shows that the sample consists primarily of the $ErNi_2B_2C$ phase. Weak diffraction peaks associated with the impurity phases ErNiBC and Ni_2B are also found. A piece of the annealed button of mass 7–9 g is then placed on the top of an equal mass of Ni_2B pieces inside a 5 ml alumina crucible. These are put into a vertical tube furnace under flowing high-purity (99.9%) argon and heated according to the time and temperature schedule shown in Fig. 1. The purpose of the initial soak at 200 °C is to flush the oxygen from the system. The sample is then heated to 1490 °C. The slow heating from 1475 to 1490 °C allows the Ni_2B flux to incorporate as much of the $ErNi_2B_2C$ as possible and serves to homogenize the melt. In addition, since the vertical tube furnace used has a maximum temperature of 1500 °C, this slow ramp prevents overshooting the maximum temperature. The crystals grow during the cooling step from 1490 to 1200 °C over 60 h. The furnace is then shut off and allowed to cool to room temperature over approximately 12 h. The platelike crystals are then removed from the excess flux. Crystals as large as 500 mg (7 mm × 7 mm × 0.5 mm) can be grown. The large surface of the plates is normal to the crystallographic c axis. Cooling for longer times has not significantly increased crystal size and growth of crystals larger than 1 g will probably require either larger crucibles or a different growth method.

Not all of the original polycrystalline $ErNi_2B_2C$ button is incorporated into the melt during the growth process. When the growth cycle is completed, part of the button is still above the surface of the flux. Some of the flux has wicked up into this part of the original button and has led to greatly enhanced grain growth of relatively large, highly intergrown crystals. The presence of this partially reacted button seems to be important since growths using smaller mass ratios of $ErNi_2B_2C$ to Ni_2B generally yield smaller crystals. We find that flux-grown crystals nucleate on two different types of sites: nucleation on the partially reacted $ErNi_2B_2C$ button that is in contact with the flux, and nucleation on the surface of the Al_2O_3 crucible, well removed from the unreacted part of the $ErNi_2B_2C$ button. In general, the crystals that nucleate on the crucible are the larger, better formed ones.

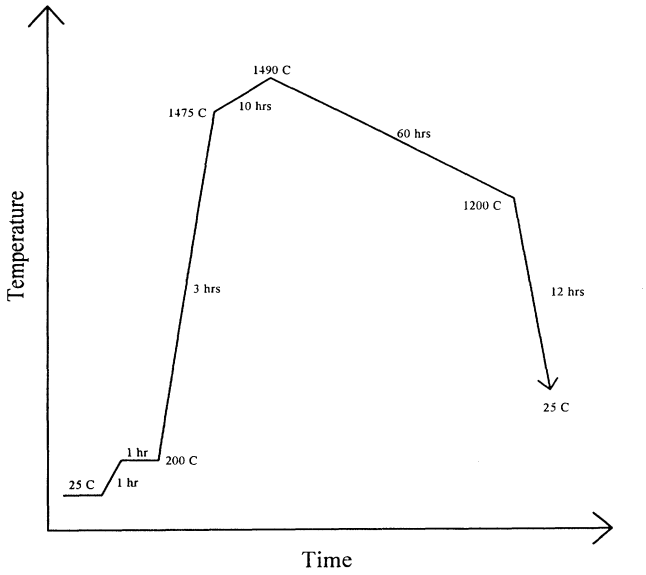

FIG. 1. Temperature and time schedule for the growth of single crystals of $ErNi_2B_2C$. The starting sample is a button of stoichiometric polycrystalline $ErNi_2B_2C$ prepared by arc melting, and placed in an Al_2O_3 crucible with an equal mass of Ni_2B.

Powder x-ray-diffraction patterns of pulverized single crystals show the crystals to be single phase [only the most intense (2,1,1) line of Ni_2B was seen and is due to small amounts of flux remaining on the surface of the crystal]. The other peaks seen in the initial polycrystalline arc-melted sample as second phases are no longer present in the powder x-ray-diffraction patterns of the crushed single crystal. It should be noted here that separate magnetic measurements of Ni_2B do not reveal any phase transitions for 2 K $< T <$ 300 K and show Ni_2B to be a Pauli paramagnet over this whole temperature range. Neutron-scattering measurements show that the crystals grown using this method are of high quality with a small mosaic spread of less than 0.1°.[14]

A crystal of mass 12 mg with clean surfaces was selected for magnetization measurements. A rectangular parallelepiped crystal with dimensions 4 mm × 1 mm × 0.17 mm for magnetoresistance measurements was cut out of a larger crystal using a wire saw. The temperature

and magnetic field (H) dependences of the static magnetization were measured using a Quantum Design superconducting quantum interference device (SQUID) magnetometer. A Linear Research Inc. LR400 four-wire ac resistance bridge was used in conjunction with the T and H environmental control of the SQUID magnetometer to measure the in-plane four-probe resistivity as a function of temperature, field, and crystal orientation relative to the field. Gold wires 0.003 inches in diameter were attached to the surface of a crystal with Epotek H20E silver epoxy. The contact resistance was less than 1 Ω and no indications of Joule heating were detected upon varying the current density by a factor of 30. The resistivity data presented in this paper were measured with current density of ~ 1.76 A/cm^2. The specific heat of a crystal of mass ≈ 20 mg was measured from 2 to 20 K. A thermal relaxation technique[17] was used with the sample attached to a thermometer/heater diamond platform by a small amount of Apiezon grease. The specific-heat data were corrected for an additive term due to the addenda, the contribution of which was determined by a separate measurement, and the accuracy of these measurements is about 1%.

III. EXPERIMENTAL RESULTS AND ANALYSIS

A. Specific-heat measurement

Figure 2 displays the temperature-dependent specific-heat data, $C_p(T)$ for 2 K $< T <$ 20 K. There is a clear lambda-shaped anomaly with a peak at (5.85±0.15) K that can be associated with the transition of the Er sublattice from paramagnetism to antiferromagnetic order.[14,18] Another measurement on a different crystal (not shown) yielded the same T_N as for the first crystal, to within the error bars. These measurements were carried out in zero applied field (H). The electronic and lattice terms of the specific heat for $HoNi_2B_2C$ are also plotted as the solid curve in Fig. 2 using $C_p(T)=\gamma T+\beta T^3$ where $\gamma=20$ mJ/mol K^2 and $\beta=0.35$ mJ/mol K^4.[8] For temperatures higher than 11 K, the $C_p(T)$ data increase with increasing temperature at a much faster rate than would be anticipated from the γ and β values from $HoNi_2B_2C$. This is probably due to a Schottky anomaly associated with crystalline electric-field (CEF) levels split from the ground state by roughly 50–60 K. Due to this low-lying Schottky anomaly it is difficult to evaluate the entropy associated with the magnetic phase transition at 6 K precisely. The magnetic entropy at 6 K is 10.5 J/mol K which can be consistent with either a three- or fourfold degenerate state ordering at 6 K. The negative slope of $C_p(T)$ from T_N up to ≈ 10 K is indicative of pretransitional magnetic fluctuations, which would cause a reduction in the magnetic ordering entropy at T_N and increase the value of the above estimated degeneracy. There is a small feature at $T_c \approx 10.5$ K, but due to the large magnetic background the superconducting phase transition at 10.5 K is not clearly observed in the specific-heat data. This is similar to the situation found in specific-heat measurements on $HoNi_2B_2C$.[8] The origin of the apparent low-temperature shoulder in the data at $T \approx 2.2$ K is unknown.

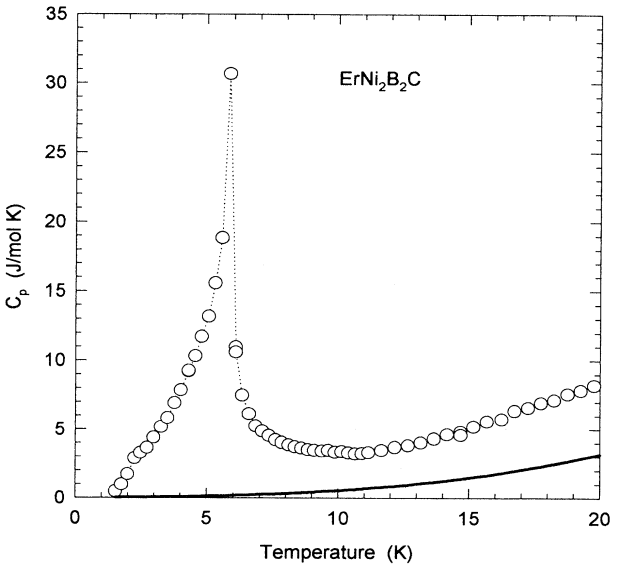

FIG. 2. Specific heat (C_p) of $ErNi_2B_2C$ versus temperature (open circles). The approximate electronic and lattice contributions to the specific heat of $ErNi_2B_2C$ are shown by the solid curve, using $C_p(T)=\gamma T+\beta T^3$ with $\gamma=20$ mJ/mole K^2 and $\beta=0.35$ mJ/mole K^4 from Ref. 8.

B. Overall temperature dependencies of the magnetization and electrical resistivity from 2 to 300 K

Typical magnetization M versus applied magnetic field H isotherm data for single-crystal $ErNi_2B_2C$ are shown in Fig. 3(a) for **H**‖**c** and Fig. 3(b) for **H**⊥**c** at several different temperatures. For both **H**‖**c** and **H**⊥**c**, the magnetizations ($M_\parallel$ and $M_\perp$, respectively) are linear in H for $T \geq 50$ K. For $T < 50$ K, $M_\parallel$ remains linear in H down to 10 K and there is almost no change in slope ($dM_\parallel/dH$). On the other hand, $M_\perp(H)$ becomes highly nonlinear for decreasing T and also becomes significantly larger than $M_\parallel$. This indicates that the magnetic anisotropy increases as T decreases and that the Er^{+3} ion moments lie mainly along the plane normal to **c** at low T.

Figure 4(a) shows the temperature-dependent anisotropic magnetization divided by applied magnetic field (M/H) of $ErNi_2B_2C$ with **H**=15 kG ⊥**c** and ‖**c** for 2 K $\leq T \leq$ 300 K; the inset shows an expanded plot of the data below 10 K. At the lowest temperatures, a large anisotropy is evident, with a much larger magnetization for **H**⊥**c** than for **H**‖**c**. This anisotropy becomes smaller as the temperature increases and changes sign at ~ 150 K, so that M is slightly smaller for **H**⊥**c** than for **H**‖**c** above 150 K. The change of sign can also be seen in $M(H)$ isotherm data. Comparison of the slopes of $M(H)$ in Fig. 3 for both **H**‖**c** and **H**⊥**c** at $T=50$, 150, and 300 K shows that $M_\parallel < M_\perp$ for $T=50$ K, $M_\parallel \approx M_\perp$ for $T=150$ K, and $M_\parallel > M_\perp$ for $T=300$ K. Figure 4(a) also shows that $M_\parallel(T)$ has a nonmonotonic temperature dependence

below ≈ 50 K and has a broad maximum around 30 K. As will be discussed later, this broad maximum reflects the occurrence of CEF levels split from the ground state by roughly 40–50 K. The sharp drop of $M_\perp(T)$ at $T_N \approx 4$ K for $H = 15$ kG results from antiferromagnetic ordering of the Er^{+3} ions, where this value of T_N is suppressed from the $T_N = 6$ K value in zero applied field. This suppression of T_N with $\mathbf{H} \perp \mathbf{c}$ will be discussed in detail below.

Figure 4(b) shows the inverse of the magnetization divided by applied magnetic field versus T for the data in Fig. 4(a), together with a calculated powder averaged one: $M_{\text{avg}}(T)/H = 2M_\perp(T)/3H + M_\parallel(T)/3H$. For all three cases, the data show Curie-Weiss behavior,

$$\frac{M}{H} = \frac{C}{(T-\theta)} = \frac{N\mu_{\text{eff}}^2}{3k_B(T-\theta)} , \quad (1)$$

for the high-temperature region 200 K $\leq T \leq$ 300 K. Fitting Eq. (1) to the data for T $\geq$200 K in Fig. 4(b) yields $\mu_{\text{eff}} = (9.30 \pm 0.05)\mu_B$, $(9.50 \pm 0.05)\mu_B$, and $(9.40 \pm 0.05)\mu_B$ for $\mathbf{H} \perp \mathbf{c}$, $\mathbf{H} \| \mathbf{c}$, and the powder average, respectively. These values are all close to the theoretical value of $\mu_{\text{eff}} = 9.59\mu_B$ for the Hund's Rule ground state of the isolated Er^{+3} ion. The Weiss temperatures are found to be $\theta_\perp = (-7.4 \pm 0.6)$ K, $\theta_\parallel = (-5.7 \pm 0.7)$ K, and (-6.8 ± 0.8) K for $\mathbf{H} \perp \mathbf{c}$, $\mathbf{H} \| \mathbf{c}$, and the powder average, respectively.

Figure 4 also shows that a large deviation from the high-temperature Curie-Weiss behavior of the Er^{+3} ions occurs below 100 K for $\mathbf{H} \| \mathbf{c}$, indicating that their magnetic state changes dramatically below this temperature. In contrast, the $1/\chi_{\text{avg}}$ vs T data are linear over the much wider temperature range, 10 K $\leq T \leq$ 300 K, effectively concealing this anisotropy. Similar anisotropies of $\chi(T)$ and the free-ion-like Curie constant of $1/\chi_{\text{avg}}(T)$ have been observed in $HoNi_2B_2$ (Ref. 8) and $TmNi_2B_2$ (Ref. 10) and are also attributed to crystalline electric-field (CEF) effects. For the tetragonal point symmetry ($I4/mmm$) of an R ion in the RNi_2B_2C compounds, five nonzero terms occur in the CEF Hamiltonian,[19]

$$H_{\text{CEF}} = B_2^0 O_2^0 + B_4^0 O_4^0 + B_4^4 O_4^4 + B_6^0 O_6^0 + B_6^4 O_6^4 , \quad (2)$$

where O_n^m are Stevens operators. In many cases the $B_2^0 O_2^0$ term is dominant. Thus an initial estimation of the value of B_2^0 is important in analyzing the anisotropic $\chi(T)$ in a CEF scheme. This can be done by using the equation[20]

$$B_2^0(\text{K}) = \frac{10}{3(2J-1)(2J+3)}(\theta_\perp - \theta_\parallel) . \quad (3)$$

By substituting the above values $\theta_\perp = (-7.4 \pm 0.6)$ K,

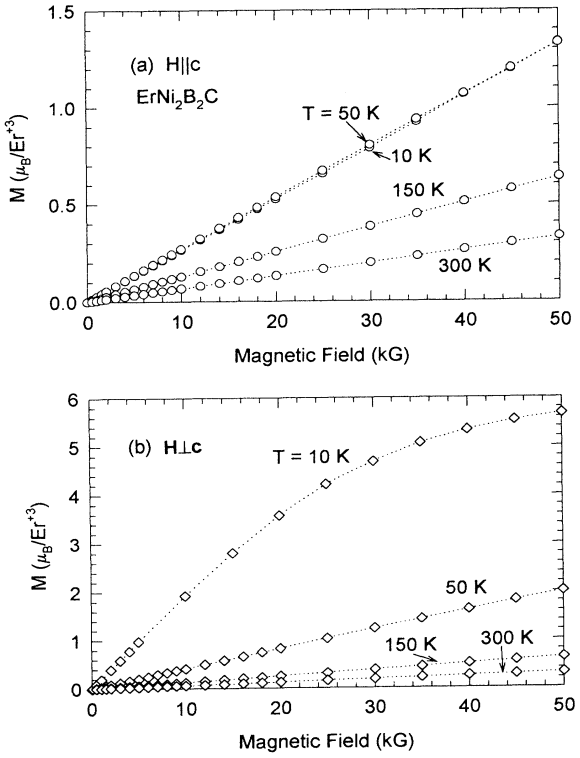

FIG. 3. Magnetization M versus applied magnetic field for an $ErNi_2B_2C$ crystal for several different temperatures (a) for $\mathbf{H} \| \mathbf{c}$ and (b) for $\mathbf{H} \perp \mathbf{c}$.

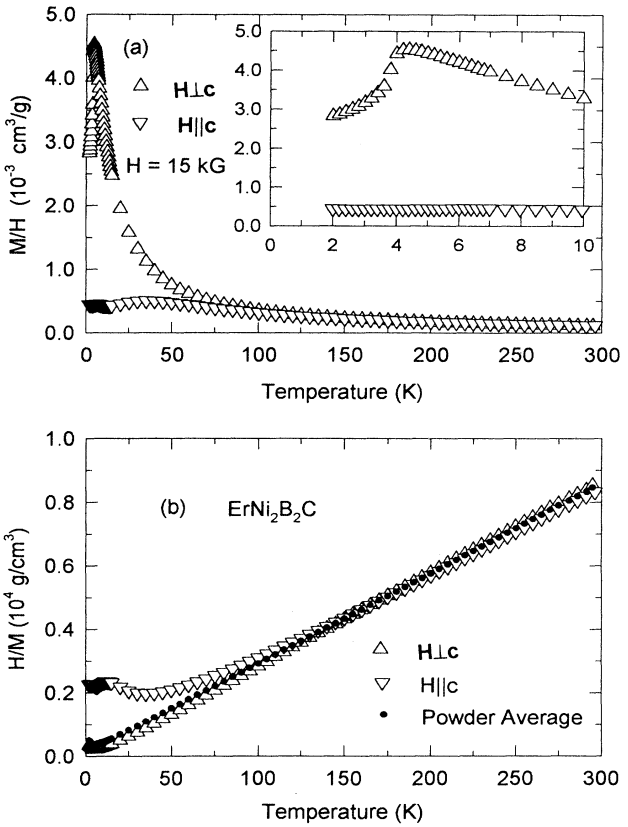

FIG. 4. (a) Anisotropic magnetization divided by applied magnetic field M/H versus temperature T for an $ErNi_2B_2C$ crystal for 2 K $\leq T \leq$ 300 K. Inset: Low-temperature data plotted on an expanded scale. (b) Inverse of M/H vs T for an $ErNi_2B_2C$ crystal, obtained from the data in (a). The closed circles represent $(M/H)^{-1}$ for a powder average of the M/H data for $\mathbf{H} \| \mathbf{c}$ and $\mathbf{H} \perp \mathbf{c}$.

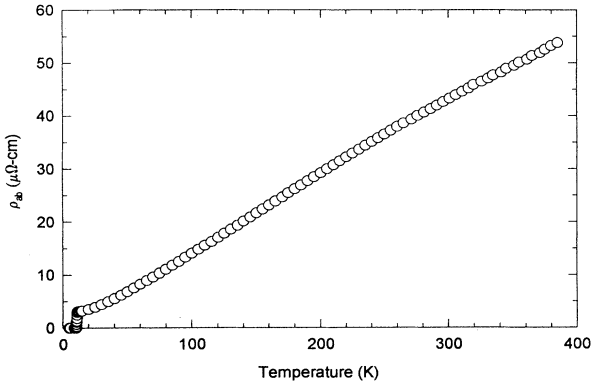

FIG. 5. Electrical resistivity in the *ab* plane ρ_{ab} versus temperature for an $ErNi_2B_2C$ crystal.

$\theta_{\parallel}=(-5.7\pm0.7)$ K, and $J=15/2$ for the Er^{+3} ion in $ErNi_2B_2C$, we obtain $B_2^0=(-0.022\pm0.017)$ K. The above equation for B_2^0 is derived from the expansion of magnetic susceptibility $\chi(T)$ as a power series in $1/T$ for free ions under a CEF, not including the interatomic exchange effects. Thus the value of B_2^0 derived here can be used as a starting value for a more detailed analysis of the anisotropic $\chi(T)$ which also takes the rare-earth ion interactions into account.

The temperature dependence of the in-plane resistivity (ρ_{ab}) for 2 K $\leq T \leq$ 400 K is shown in Fig. 5. The high quality of the single crystal can be seen by the large value of the residual resistivity ratio, $\rho_{ab}(400\text{ K})/\rho_{ab}(10\text{ K})\approx 18$, and by the absolute resistivity value just above T_c, 3.5 $\mu\Omega$ cm, which is lower than the values previously reported for polycrystalline samples.[16] For comparison, the average temperature coefficient of resistivity $d\rho_{ab}/dT\approx 0.15$ $\mu\Omega$ cm/K for $50\leq T<400$ K, which is much smaller than $d\rho/dT$ for polycrystalline $LuNi_2B_2C$, but comparable to that for polycrystalline $TmNi_2B_2C$.[5] The overall temperature dependence of ρ_{ab} appears to be slightly nonlinear. The shape of $\rho_{ab}(T)$, i.e., the negative curvature from $\approx$150 K to our high-temperature limit of 400 K, is reminiscent of the $\rho(T)$ of the *A*-15 structure compounds like Nb_3Sn.[21] There, the saturation of ρ with increasing T was attributed to a strong electron-phonon interaction which decreased the mean free path to interatomic distances at high T. Specific-heat measurements performed on $LuNi_2B_2C$ (Ref. 22) and YNi_2B_2C (Ref. 23) gave linear heat-capacity coefficients $\gamma=11\sim19$ mJ/mole K^2. From this γ and the $\rho_{ab}(400\text{ K})$ value in Fig. 4, the electron relaxation time (τ) in the Drude model of free electrons is estimated to be $(7.9\pm2)\times10^{-16}$ sec. Using the reported Fermi velocity ($v_{Fx}=v_{Fy}=2.12\times10^7$ cm/sec) from band-structure calculations,[7] the mean free path at $T=400$ K is calculated to be (1.7±0.4) Å which is comparable with the interatomic distance (1.5~3 Å), and consistent with the above scenario.

C. Magnetization and resistivity measurements below 12 K

The M/H versus T data for 2 K $<T<12$ K are shown in Figs. 6(a) and 6(b) for several values of **H**⊥**c** and **H**∥**c**, respectively. For **H**⊥**c** the data follow a Curie-Weiss temperature dependence at higher temperature and gradually show a negative deviation from this as temperature is lowered. For **H**⊥**c**=2 kG, this happens near 10 K and for **H**⊥**c**=5 kG, this happens at approximately 8 K. We believe that this negative deviation from the Curie-Weiss law is due to the onset of superconductivity (see below). Since the magnetization of the Er^{+3} sublattice for **H**⊥**c** is large compared with the superconducting magnetization, the determination of T_c from the $M(T)$ data for this field direction is not definitive. For **H**∥**c**, the T_c can be determined more clearly than for **H**⊥**c** due to the smaller background magnetization of the Er^{+3} sublattice, but this extraction of $T_c(H)$ is only definitive for $H<8$ kG. As will be shown below, these values of T_c (for H less than 5 kG for **H**⊥**c** and less than 10 kG for **H**∥**c**) agree well with values determined from magnetoresistance data taken under identical field conditions.

The antiferromagnetic transition temperature T_N can be determined from the maximum in $d(MT)/HdT$.[8,24] Using this criterion, $T_N=6.0$ K for **H**⊥**c**=2 kG, which is in agreement with the specific-heat data shown in Fig. 2 and with magnetic neutron-diffraction results at $H=0$.[14,15] As can be seen in Fig. 6(a), T_N decreases with increasing H for **H**⊥**c**. For **H**∥**c**, the temperature-dependent magnetization is significantly different than for

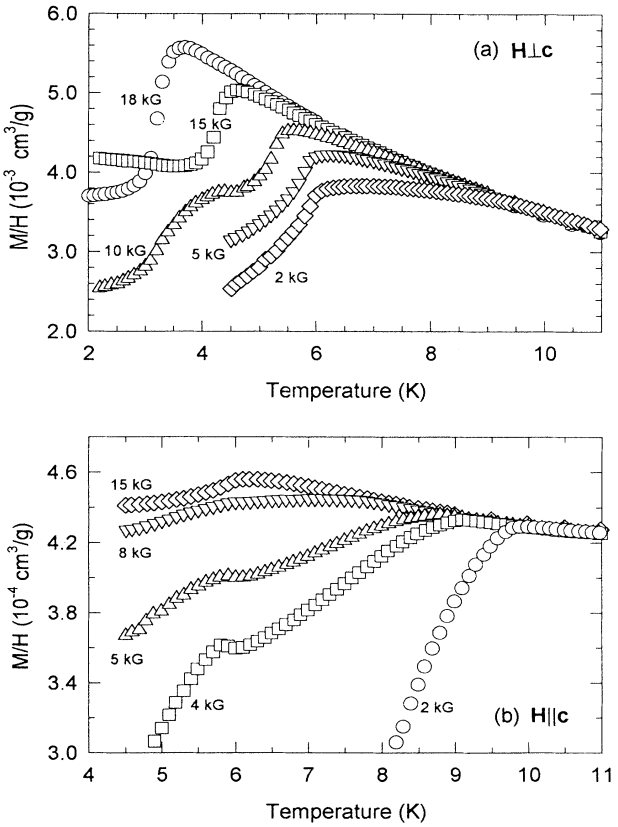

FIG. 6. Magnetization divided by applied magnetic field M/H, for various magnetic fields, versus temperature for (a) **H**⊥**c** and (b) **H**∥**c**.

H⊥c. The AF ordering of the Er^{3+} ions is manifested by a small kink in the superconducting diamagnetic $M(T)$ data. Furthermore, in contrast to $T_N(H)$ for H⊥c, T_N is seen to be nearly independent of H for $H < 15$ kG. These dependences of $T_N(H)$ for H||c and H⊥c, determined from the data in Fig. 6, are plotted as the filled symbols in Fig. 7.

The high-field magnetization data for H⊥c are plotted in Fig. 8. At $T = 2$ K the $M(H)$ data, taken with increasing H, exhibit a metamagnetic transition near 12 kG for H⊥c. The magnetic moment in this region is $\approx 3.5\mu_B$ per formula unit. A second field-induced transition to a nearly saturated magnetic state is seen for $H \approx 20$ kG, where the saturation magnetic moment at 50 kG is $8.4\mu_B$ per Er, which is 93% of the saturation moment of a free Er^{+3} ion. In addition to these two easily observed field-induced transitions, $ErNi_2B_2C$ also shows two weak field-induced transitions at $T = 2$ K for $H \approx 1$ and 7 kG, appearing as small inflections in the $M(H)$ data. These latter two transitions disappear by $T = 4.5$ K and are of unknown origin. For $T = 4.5$ K there is a change in slope in the $M(H)$ data for $H \sim 12$ kG. This may be a broadened form of the metamagnetic phase transition seen at this field at $T = 2$ K or may be a transition out of the AF ordered state associated with suppressing T_N to below 4.5 K. This latter hypothesis is consistent with Fig. 7 and neutron-diffraction data collected in applied field.[14,18] From Fig. 8 no obvious field-induced transitions are seen at 2 K for H||c and $H \leq 50$ kG. The occurrence of field-induced magnetic transitions for H⊥c and the lack of them for H||c are similar to the behavior observed in $HoNi_2B_2C$.[8]

The superconducting transitions as measured by low-field ($H = 10$ G) magnetization and zero-field resistivity measurements are plotted in Figs. 9(a) and 9(b), respectively. From Fig. 9(a), the onset of the superconducting diamagnetism appears at $T = 10.5$ K and 90% of the full diamagnetic magnetization is reached at $T = 10$ K. The resistivity data in Fig. 9(b) show a superconducting onset at a higher temperature of 11.3 K and zero resistivity at $T = 10.5$ K. A comparison of the two measurements shows that the zero-resistivity temperature corresponds to the onset temperature of the superconducting magnetization, implying that the initial decrease of resistivity with decreasing temperature in the $ErNi_2B_2C$ crystal may be due to some sort of filamentary superconductivity. When using electrical resistivity data, zero resistivity will henceforth be used as the criterion to determine T_c.

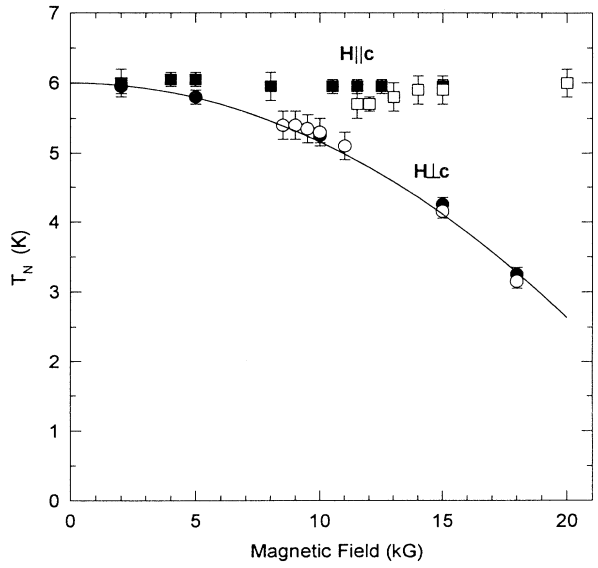

FIG. 7. Néel temperature T_N versus applied magnetic field, from magnetization data (filled symbols) and from resistivity data (open symbols): H||c (squares) and H⊥c (circles). The solid curve is a fit to the H⊥c data of the expression $T_N = T_0 - AH^2$, with $T_0 = 6.03$ K and $A = 8.3 \times 10^{-9}$ K/G^2.

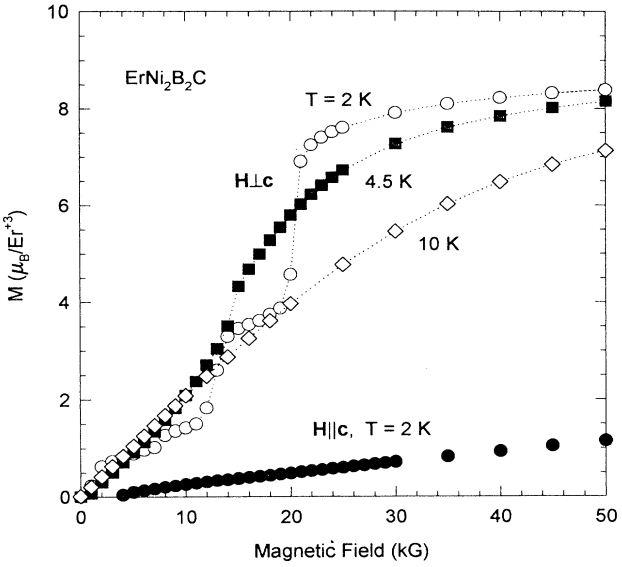

FIG. 8. Magnetization M versus applied magnetic field for an $ErNi_2B_2C$ crystal at the indicated temperatures for H⊥c and H||c.

Magnetoresistivity $\rho_{ab}(H,T)$ measurements for H⊥c [Fig. 10(a)] and H||c [Fig. 10(b)] show large anisotropies. For H⊥c, T_c decreases with increasing H as expected and there is no change in the zero-resistance state near $T_N = 6$ K (see Fig. 7) for $H \leq 8$ kG. For 8.5 kG $\leq H \leq 10$ kG, T_c has decreased to $\approx T_N$, the transition width increases significantly, and the effect of the AF ordering on superconductivity appears as a small kink within the superconducting transition temperature region. Reentrant behavior is not found at any field for H⊥c. The effect of AF ordering on the normal-state resistivity is also displayed for $H = 15$ and 18 kG as a slope change (marked by vertical arrows) due to the reduction of spin-disorder scattering of conduction electrons. A decrease of T_N with increasing field can be clearly seen in Fig. 10(a).

The $\rho_{ab}(T,H)$ data for H||c in Fig. 10(b) show a decrease of T_c with increasing field similar to, but slower than, the decrease for H⊥c in Fig. 10(a) for $H < 10$ kG. At $H = 11$ kG, the resistivity reaches zero at 6.6 K and a

small nonzero resistivity reappears at 6 K. The resistivity returns to zero below 5 K and remains zero to 2 K, the lowest temperature attainable. This reentrant behavior of the magnetoresistivity manifests itself more clearly at $H=12$ kG: zero resistance is seen between 6.4 and 6.0 K, nonzero resistance between 6.0 and 4.6 K, and zero resistance again below 4.6 K. For $H \geq 13$ kG, the effect of AF ordering can be seen as an S-shaped feature in $\rho_{ab}(T)$ near 6 K which smears out as the field increases above 15 kG. For $H=20$ kG (above H_{c2}), the normal-state resistivity shows slope changes at two different temperatures. The first drop of resistivity at 6 K is attributed to the AF ordering of the Er^{+3} magnetic sublattice and the second one near 3 K is of unknown origin.

The Néel temperature T_N can be determined from the resistivity data as the temperature of the local maximum in $\rho_{ab}(T,H)$ for $H \leq H_{c2}$ and the onset temperature of slope change in $\rho_{ab}(T,H)$ for $H \geq H_{c2}$. For the $\mathbf{H}\|c$ data shown in Fig. 10(b), these criteria evolve into each other smoothly. The $T_N(H)$ dependences for $\mathbf{H}\|\mathbf{c}$ and $\mathbf{H}\perp\mathbf{c}$ found from the data in Fig. 10 are plotted in Fig. 7, where good agreement with the respective $T_N(H)$ dependences found from the $M(H,T)$ measurements is seen.

In order to better understand the reentrant superconducting behavior seen for the intermediate fields in Fig. 10(b), we measured the resistivity versus field isotherms between 5 and 7 K for both $\mathbf{H}\perp\mathbf{c}$ [Fig. 11(a)] and $\mathbf{H}\|\mathbf{c}$ [Fig. 11(b)]. The temperature-dependent upper critical magnetic field, $H_{c2}(T)$, determined from these isotherms [as well as $H_{c2}(T)$ data from Figs. 6 and 10] are plotted in Fig. 12. For $\mathbf{H}\perp\mathbf{c}$, the resistivity remains near zero for $H \leq 8$ kG and becomes nonzero between 8 and 9 kG for the five temperatures between 5 and 6 K shown. The resistivity data at 9 kG increase with T from 5 to 6 K, which means that the magnetic field at which nonzero resistivity starts to appear, defined here as $H_{c2}(T)$, is between 8 and 9 kG and continuously decreases from 5 to 6 K (see Fig. 12). Thus there is no local minimum in $H_{c2}(T)$ between 5 and 6 K, which is consistent with the measurements of resistivity versus temperature. In other words, the lack of reentrant superconductivity for $\mathbf{H}\perp\mathbf{c}$ precludes a local minimum in $H_{c2}(T)$. Figure 11(b) shows the resistivity versus field for $\mathbf{H}\|\mathbf{c}$ at seven different temperatures near T_N. In contrast to $\mathbf{H}\perp\mathbf{c}$, the $H_{c2}(T)$ for $\mathbf{H}\|\mathbf{c}$ is not a monotonic function of temperature between 5 and 7 K. The $H_{c2}(T)$ data decrease from 11.5 kG at 5 K to 11 kG at 5.5 K and then remain almost constant up to 5.8 K. The $H_{c2}(T)$ then increases to between 11 and 12 kG at 5.9 K and reaches a maximum of 12 kG at 6 K. Above 6 K, $H_{c2}(T)$ decreases monotonically with temperature with $H_{c2}(7\text{ K})$ being between 9 and 10 kG (see Fig. 12). Thus, these $\rho_{ab}(H,T)$ data for 5 K $\leq T \leq 7$ K show clear evidence of a local minimum in $H_{c2}(T)$ just below T_N, consistent with the reentrant behavior in the $\rho_{ab}(T)$ data in Fig. 10.

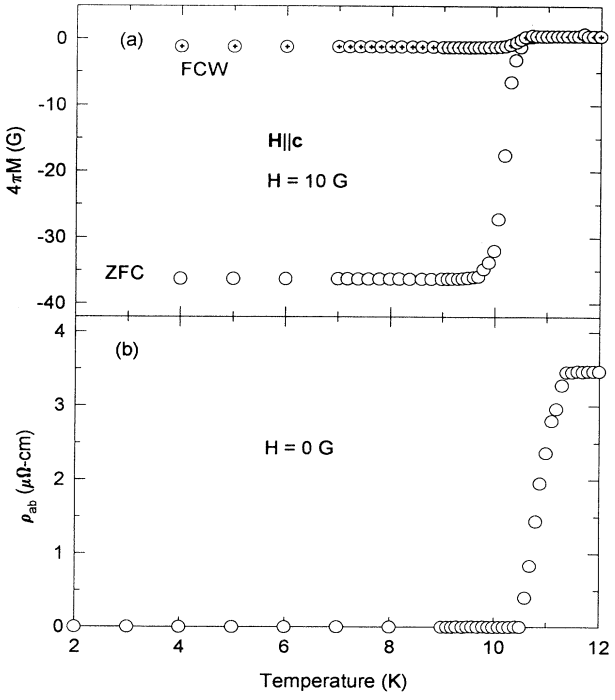

FIG. 9. (a) Volume magnetization M in an applied field $H=10$ G versus temperature for an $ErNi_2B_2C$ crystal for $\mathbf{H}\|\mathbf{c}$: zero-field-cooled (ZFC) (open circles) and field-cooled (FCW) (circles with crosses) data taken on warming as shown. (b) Electrical resistivity in the ab plane ρ_{ab} versus temperature for zero applied field.

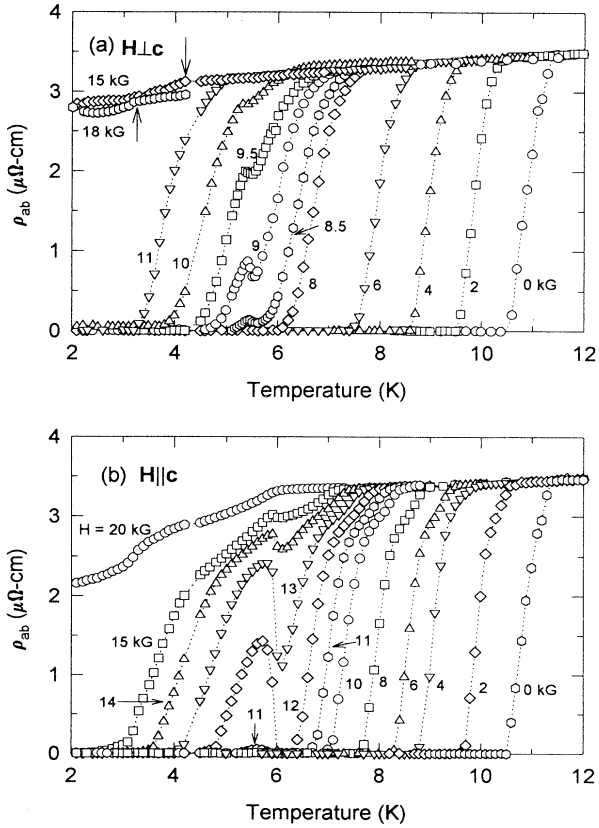

FIG. 10. Electrical magnetoresistivity in the ab plane ρ_{ab} versus temperature with (a) $\mathbf{H}\perp\mathbf{c}$ and (b) $\mathbf{H}\|\mathbf{c}$ at the indicated applied magnetic field H values.

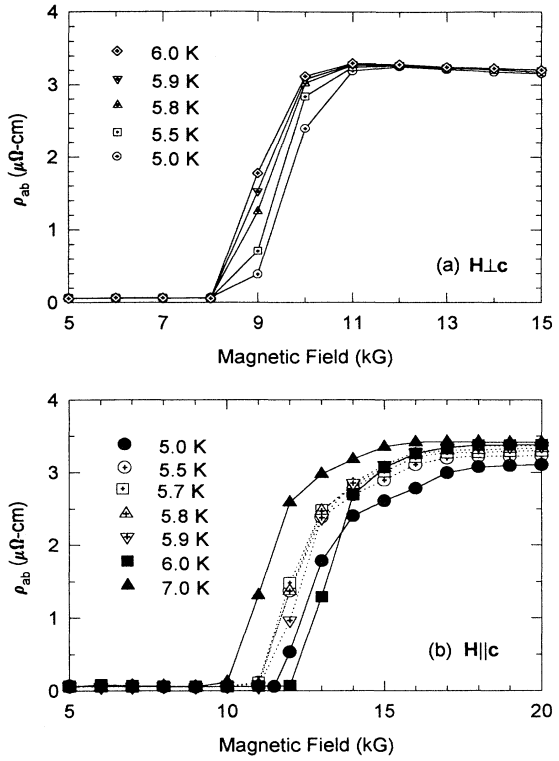

FIG. 11. Electrical resistivity of an $ErNi_2B_2C$ crystal in the *ab* plane ρ_{ab} versus applied magnetic field H at several temperatures for (a) **H⊥c** and (b) **H||c**.

The variation of the normal-state resistivity as a function of temperature at 15 kG for **H⊥c** [Fig. 11(a)] and at 20 kG for **H||c** [Fig. 11(b)], i.e., above H_{c2}, can be qualitatively explained by magnetic scattering of conduction electrons. The variation of resistivity at 20 kG [$\Delta\rho_{ab}=\rho_{ab}(6\text{ K})-\rho_{ab}(5\text{ K})$] for **H||c** is about 0.3 $\mu\Omega$ cm which is much larger than that for **H⊥c** ($\Delta\rho_{ab}\leq 0.1\mu\Omega$ cm). For **H||c**, long-range AF ordering occurs at 6 K and lowers the resistivity due to the reduction of the magnetic scattering. On the other hand, T_N for **H⊥c** is shifted down to 4 K at $H=15$ kG (see Fig. 6), resulting in no reduction of magnetic scattering in the temperature region examined.

The magnetoresistivity of $ErNi_2B_2C$ at 2 K is plotted in Figs. 13(a) and 13(b) for **H||c** and **H⊥c** for fields up to $H=50$ kG, respectively. For **H||c**, the sharp increase of resistivity at $H\approx 15$ kG is the transition from the superconducting state to the normal state, i.e., $H_{c2}(2\text{ K})\approx 15$ kG. For **H⊥c**, the critical field is seen to be $H_{c2}(2\text{ K})=12.3$ kG. The $\rho_{ab}(H)$ data for **H⊥c** show clear hysteresis between increasing and decreasing fields near H_{c2}, indicating a first-order superconducting transition, and also above H_{c2}. For **H⊥c**, the H_{c2} value coincides with

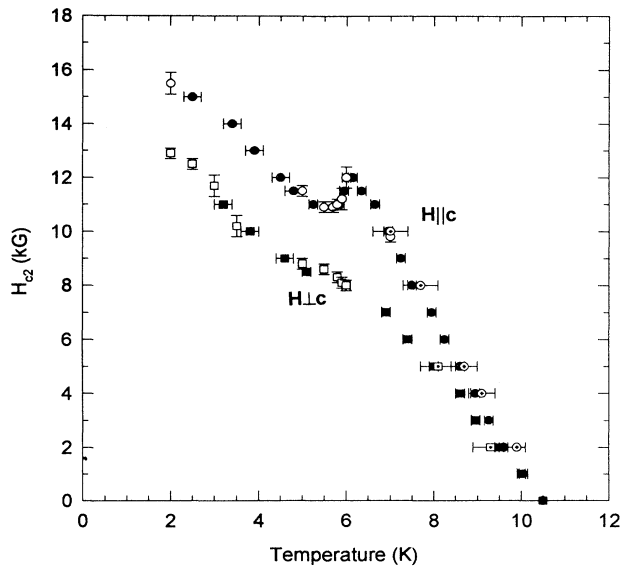

FIG. 12. Upper critical magnetic field H_{c2} versus temperature for single crystal $ErNi_2B_2C$, with **H||c** (circles) and **H⊥c** (squares): H_{c2} deduced from $\rho_{ab}(T)$ (closed symbols), $\rho_{ab}(H)$ (open symbols), and $M(T)$ (symbols with cross) measurements.

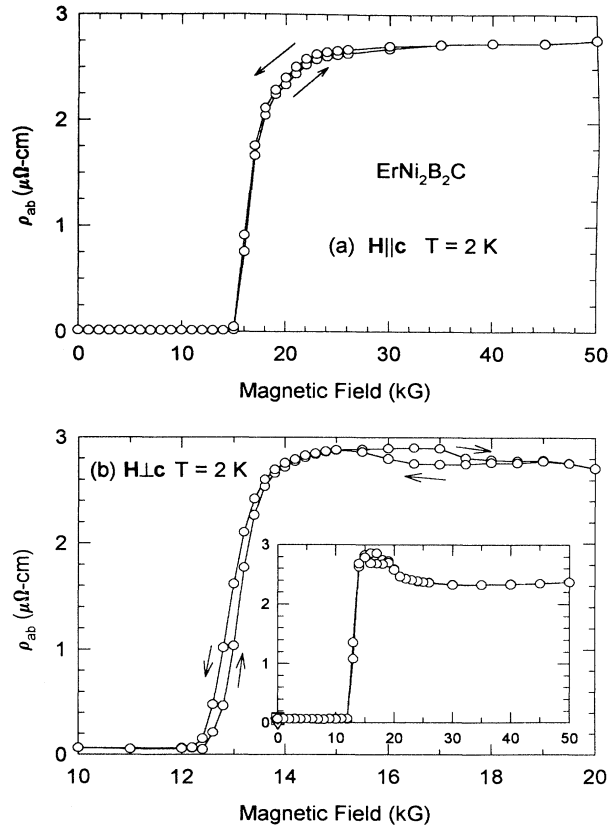

FIG. 13. Electrical resistivity of an $ErNi_2B_2C$ crystal in the *ab* plane ρ_{ab} versus applied magnetic field H at $T=2$ K with (a) **H||c** and (b) **H⊥c**. The arrows indicate increasing and decreasing field. Inset of (b): extended temperature scale.

the field at which the metamagnetic transition occurs (see Fig. 8), suggesting that the metamagnetic state is detrimental to superconductivity. The second higher-field hysteretic region for $\mathbf{H}\perp\mathbf{c}$ is associated with the magnetic transition to the field-induced nearly saturated paramagnetic state which is therefore apparently also first order. Above $\sim$20 kG [inset to Fig. 13(b)], the negative slope of the magnetoresistivity is presumably due to a reduction in spin-disorder scattering as magnetic saturation is approached.

IV. DISCUSSION

It is very interesting to compare the magnetic and superconducting properties of $ErNi_2B_2C$ determined here with those of the (Ho,Tm)Ni_2B_2C compounds. The magnetic anisotropy of the normal state in $ErNi_2B_2C$ shows quite different behavior from those of (Ho,Tm)Ni_2B_2C. For the latter two compounds, the sign of the anisotropy does not change over the whole temperature range 10 K $\leq T \leq$ 300 K, i.e., $\chi_\perp(T) > \chi_\parallel(T)$ for $HoNi_2B_2C$ (Ref. 8) and $\chi_\perp(T) < \chi_\parallel(T)$ for $TmNi_2B_2C$.[10] As shown in Fig. 4 for $ErNi_2B_2C$, there is a crossover at $T \approx 150$ K, such that $\chi_\perp(T) > \chi_\parallel(T)$ for $T < 150$ K, and $\chi_\perp(T) < \chi_\parallel(T)$ for $T > 150$ K. We believe that the CEF interaction is responsible for the normal-state anisotropy in these RNi_2B_2C materials and the CEF parameter B_2^0, estimated above to be (-0.022 ± 0.017) K, plays a key role in determining the easy-axis direction. This parameter can be written as[25]

$$B_2^0 = \langle r^2 \rangle A_2^0 \alpha_J ,$$

where $\langle r^2 \rangle$ is the mean-square radius of the $4f$ electrons, A_2^0 represents the electrostatic effects from the static charges of the lattice of neighboring ions, and α_J is the Stevens multiplicative factor.[18] Assuming that A_2^0 has a sign independent of the particular rare-earth element among an isostructural series of compounds, and since the radial integral is positive by definition, the sign of B_2^0 depends only on the sign of α_J, which is positive for Ho^{+3} and negative for Er^{+3} and Tm^{+3}.[25] This then gives nice agreement with the observed sign change from positive $B_2^0 \approx 0.85$ K for $HoNi_2B_2C$ (Ref. 26) to negative $B_2^0 \approx -1.15$ K for $TmNi_2B_2C$ (Ref. 10) and (-0.022 ± 0.017) K for $ErNi_2B_2C$. The direction of the easy axis, in general, depends upon the sign of B_2^0, as in the hexagonal RCo_5 and R_2Co_{17} (Ref. 27) and tetragonal RRh_4B_4 series of compounds,[28] and in $HoNi_2B_2C$ (Ref. 26) and $TmNi_2B_2C$.[10] However, this correlation is expected only when $B_2^0 O_2^0$ is the dominant term in the CEF Hamiltonian, as in most cases mentioned above. In $ErNi_2B_2C$, the magnitude of B_2^0 is much smaller than either of those for $HoNi_2B_2C$ or $TmNi_2B_2C$, so it is likely that the higher-order terms in Eq. (2) cause the crossover in the $\chi_\parallel$ and $\chi_\perp$ versus T curves near 150 K shown in Fig. 4. Quantitative calculations of the B_n^m coefficients of the RNi_2B_2C compounds are in progress.

The effects of CEF splitting of the ground state $J = 15/2$ multiplet are also manifest in the low-temperature specific heat (C_p) data for $ErNi_2B_2C$. The specific heat shows an AF transition at $T_N \approx 5.9$ K and a magnetic entropy at 6.0 K of 10.5 J/mol K which can be consistent with either a three- or fourfold degenerate state ordering at 5.9 K. In addition to this low-temperature multiplet, the rapid increase in the specific-heat data for 11 K $< T <$ 20 K is consistent with another CEF level situated at 50–60 K, giving rise to a Schottky anomaly with a peak at 20–30 K. Having CEF levels at $T = 50$–60 K is also consistent with the low-field, temperature-dependent magnetization [$M(T)$] data for $\mathbf{H}\parallel\mathbf{c}$ which show a broad maximum at $T \approx 30$ K. For $HoNi_2B_2C$,[8] the broad maximum in $M(T)$ for $\mathbf{H}\parallel\mathbf{c}$ appears around 80 K. Detailed calculations[26] of the CEF energy levels in $HoNi_2B_2C$ show that several levels split by $\sim$100 K from the ground state are responsible for the broad maximum in $M(T)$. This then is consistent with the above speculation that CEF levels split by 50–60 K from the ground state are responsible for the above features in $C_p(T)$ and $M(T)$ for $ErNi_2B_2C$.

The field dependences of T_N in single crystal $ErNi_2B_2C$ for $\mathbf{H}\perp\mathbf{c}$ and $\mathbf{H}\parallel\mathbf{c}$ are plotted in Fig. 7. While T_N for $\mathbf{H}\parallel\mathbf{c}$ is field independent, T_N for $\mathbf{H}\perp\mathbf{c}$ decreases as the field increases and becomes less than 2 K at $H = 20$ kG. These observations are consistent with the neutron-scattering measurements on single crystal $ErNi_2B_2C$,[14] which show that the intensities of the magnetic satellite peaks decrease with increasing field at 5.5 K and vanish at 10 kG for $\mathbf{H}\perp\mathbf{c}$, whereas the magnetic intensities are independent of field for $\mathbf{H}\parallel\mathbf{c}$. For $\mathbf{H}\perp\mathbf{c}$, $T_N(H)$ can be fitted by the empirical expression $T_N = T_0 - AH^2$ with $T_0 = 6.0$ K and $A = 8.3\times10^{-9}$ K/G^2, as shown by the solid curve in Fig. 7. Such a field dependence of T_N is not unique in $ErNi_2B_2C$ and similar behaviors have been observed in $HoNi_2B_2C$ (Ref. 8) and in the compound $NdRh_2Si_2$,[29] which has a tetragonal ($I4/mmm$) structure and a collinear antiferromagnetic AFI-type structure. For both $ErNi_2B_2C$ and $HoNi_2B_2C$, T_N is suppressed more rapidly for the field direction that couples more easily to the magnetic sublattice, i.e., for the low-temperature easy axis. It should be noted that measurements on polycrystalline samples would yield broadened magnetic phase transitions since the data would be an average over all crystallographic orientations.

At $T = 2$ K there are a series of metamagnetic transitions seen in the $M(H)$ data (Fig. 8). These occur over finite field regions and divide the low-temperature part of the H-T phase diagram into several regions: antiferromagnetic for $H <$ 11 kG, a transitional region for 11 kG $< H <$ 14 kG, first metamagnetic region for 14 kG $< H <$ 19 kG followed by a second transition region for 19 kG $< H <$ 22 kG, and a ferromagnetic region for $H >$ 22 kG. These regions do not appear to exist for $T \geq 4.5$ K and it is not clear how they evolve between 2 and 4.5 K. In addition to these transitions, there exist two more weaker transitions at $H \approx 1$ and 7 kG which we observed at 2 K. Detailed field-dependent magnetic neutron-diffraction measurements on single crystals are needed in order to more fully understand the details of the $ErNi_2B_2C$ magnetic phase diagram at low temperatures.

Figure 12 shows H_{c2} versus T for both field orientations based on the three different types of measurements, M vs T, ρ_{ab} vs H, and ρ_{ab} vs T. The H_{c2} values from the three different methods agree nicely in the overlapping temperature and field regions. While the overall magnitude and temperature dependences of $H_{c2}(T)$ are qualitatively consistent with those determined from ρ vs T for a polycrystal sample,[16] Fig. 12 exhibits interesting anisotropy between $\mathbf{H}\|\mathbf{c}$ and $\mathbf{H}\perp\mathbf{c}$, which shows larger H_{c2} for $\mathbf{H}\|\mathbf{c}$ than for $\mathbf{H}\perp\mathbf{c}$. This overall anisotropy is consistent with the magnetic anisotropy $M_{\|c}<M_{\perp c}$ in the normal stat at low T (see Figs. 3 and 4), implying that magnetic pair breaking due to the Er^{+3} sublattice magnetization is suppressing $H_{c2}(T)$ from what it would have been in the absence of the local moments. Possibly more conspicuous than the overall anisotropy of the $H_{c2}(T)$ data in Fig. 12 is the remarkable anisotropy in temperature dependence between $\mathbf{H}\|\mathbf{c}$ and $\mathbf{H}\perp\mathbf{c}$. Additional magnetic pair breaking due to changes in magnetic scattering near an AF phase transition have been discussed by several researchers.[30–32] Indeed, there is a remarkable qualitative agreement between the form of $H_{c2}(T)$ for $\mathbf{H}\|\mathbf{c}$ and the previous predictions of Machida, Nokura, and Matsubara[32] for RMo_6S_8 compounds. The striking aspect of Fig. 12 is that the cusp seen in $H_{c2}(T)$ at 6 K for $\mathbf{H}\|\mathbf{c}$ is absent for $\mathbf{H}\perp\mathbf{c}$. This is probably due to the fact that this feature is associated with T_N, which is relatively field independent for $\mathbf{H}\|\mathbf{c}$ and highly field dependent for $\mathbf{H}\perp\mathbf{c}$. For example, $H_{c2}(T=6\text{ K})$ for $\mathbf{H}\perp\mathbf{c}$ is approximately 8 kG (Fig. 12). By 8 kG, T_N for $\mathbf{H}\perp\mathbf{c}$ is suppressed to approximately 5.5 K (Fig. 7). This reduction in T_N with H may be responsible for the broadened, plateaulike feature at ≈ 6 K seen in the H_{c2} data for $\mathbf{H}\perp\mathbf{c}$.

It is useful to compare the H_{c2} data in Fig. 12 with those found for $HoNi_2B_2C$. For $HoNi_2B_2C$,[8] there is a 2 kG deep minimum in H_{c2} near the commensurate AF phase transition at $T_{N_2}=5.1$ K, meaning that there is 2 kG decrease in H_{c2} from the local maximum in H_{c2} just above T_{N_2}. In a plot of $H_{c2}(T)$ for $HoNi_2B_2C$, this decrease in H_{c2} appears to be "deep" since the local maximum just above T_{N_2} is only about 2 kG. In the case of $ErNi_2B_2C$ (Fig. 12), the local minimum in H_{c2} for $\mathbf{H}\|\mathbf{c}$ is somewhat more than 1 kG lower than the local maximum of 12 kG above T_N. Thus, the magnitude of the suppression of H_{c2} for $\mathbf{H}\|\mathbf{c}$ at T_N is similar to that in $HoNi_2B_2C$ at T_{N_2}, although the percentage decrease is much smaller in $ErNi_2B_2C$. This raises the question of whether the minimum in H_{c2} for $HoNi_2B_2C$ is truly anomalously deep, or simply a manifestation of a smaller T_c/T_N ratio leading to a smaller H_{c2} near T_N. Another basic difference between $ErNi_2B_2C$ and $HoNi_2B_2C$ is that $HoNi_2B_2C$ has an incommensurate magnetic ordering with c and a modulation[12] between 6 and 5 K that might lead to an enhancement of magnetic pair breaking in $HoNi_2B_2C$ that is absent in $ErNi_2B_2C$.

From the $H_{c2}(T)$ data in Fig. 12, the $dH_{c2}/dT|_{T_c}$ values are determined to be (-1.98 ± 0.08) kG/K and (-2.6 ± 0.2) kG/K for $\mathbf{H}\perp\mathbf{c}$ and $\mathbf{H}\|\mathbf{c}$, respectively. Using the relation $H_{c2}(0)=-0.69T_c(dH_{c2}/dT)|_{T_c}$,[33] the extrapolated $H_{c2}(0)$ is estimated to be (14.7 ± 0.7) kG and (19.1 ± 1.5) kG, respectively. Of course, these extrapolated values of $H_{c2}(0)$ ignore the existence of the AF ordering below T_c, and its influence on H_{c2}. Both the anisotropy of $dH_{c2}/dT|_{T_c}$ in $ErNi_2B_2C$ and the smaller magnitude of $dH_{c2}/dT|_{T_c}$ in $ErNi_2B_2C$ compared to that (~ 3.2 kG/K) in YNi_2B_2C evidently reflect the effects of the Er^{+3} sublattice magnetization. The (extrapolated) superconducting coherence length is found to be $\xi=\sqrt{\phi_0/2\pi H_{c2}(0)}=(150\pm4)$ Å and (131 ± 6) Å for $\mathbf{H}\perp\mathbf{c}$ and $\mathbf{H}\|\mathbf{c}$, respectively. The anisotropy factor, defined as $\gamma=(dH_{c2}^{\|c}/dT|_{T_c})/(dH_{c2}^{\perp c}/dT|_{T_c})$, is (1.30 ± 0.17) and is close to one, in spite of the large anisotropy in the paramagnetic normal-state susceptibility above T_c. Using $dM_{\|}/dT|_{T_c}=(15\pm3)$ G/K from Fig. 6 and the Ginzburg-Landau (GL) relation,

$$-4\pi M_s=\frac{H_{c2}(T)-H}{(2\kappa^2-1)\beta_A}\ , \tag{4}$$

where κ is the GL parameter and $\beta_A=1.16$ is a constant, κ_c is estimated to be 8.8 ± 1.2 for $\mathbf{H}\|\mathbf{c}$, which means that $ErNi_2B_2C$ is a type-II superconductor. For $\mathbf{H}\perp\mathbf{c}$, the background magnetization from the Er^{+3} sublattice is too large for $dM/dT|_{T_c}$ to be determined, so that we could not obtain the κ_{ab} value (see Fig. 6). Using $\kappa=\lambda/\xi$, the penetration depth λ is estimated to be (1160 ± 210) Å for $\mathbf{H}\|\mathbf{c}$. The superconducting parameters are summarized in Table I of the preceding paper (Ref. 10), together with those for YNi_2B_2C and $TmNi_2B_2C$.

V. SUMMARY AND CONCLUSIONS

$ErNi_2B_2C$ crystals were grown by a flux method and examined thoroughly by specific heat, magnetization, and resistivity measurements in both the superconducting and normal states. These crystals show $T_c=10.5$ K and long-range antiferromagnetic ordering at $T_N=5.9$ K, with coexistence of superconductivity and antiferromagnetism below T_N in low applied magnetic fields. The specific-heat measurements show a lambda-shaped anomaly near 5.9 K corresponding to the known[14,15] AF ordering transition. The entropy at 6 K is consistent with the ordering of either a three- or fourfold degenerate state, although the observed pretransitional increase in $C_p(T)$, indicative of fluctuation effects, would increase this estimated degeneracy. The rapid increase of C_p for temperatures above 11 K indicates that CEF levels are split off from the ground states by ~ 50 K. A splitting of CEF levels by ~ 50 K is also supported by the existence of the broad maximum in $M_{\|c}$ near 30 K.

Our measurement of the anisotropy in the normal-state magnetic susceptibility shows a change of the easy-axis direction from parallel to the c axis for $T>150$ K to normal to the c axis (easy plane) for $T<150$ K, unlike the anisotropies in (Ho,Tm)Ni_2B_2C which do not change sign with temperature. Although this anisotropy evidently comes from the CEF splitting of the ground state

$J=15/2$ multiplet of Er^{+3}, the easy-axis direction of the Er^{+3} moments does not follow the general behavior where the sign of B_2^0 plays the key role in determining the easy-axis direction, which is seen in most anisotropic magnetic compounds containing rare-earth elements. The value of B_2^0 of $ErNi_2B_2C$ is estimated to be (-0.022 ± 0.017) K from the magnetization data for $\mathbf{H}\perp\mathbf{c}$ and $\mathbf{H}\|\mathbf{c}$. While this value of B_2^0 in $ErNi_2B_2C$ is not definitive, the magnitude of B_2^0 is much smaller than those in the compounds mentioned before and the sign is found to be negative within the measurement errors. Thus the negative sign may explain the anisotropy in the high-temperature region ($T>150$ K), with the higher-order terms in the CEF Hamiltonian overriding its importance at lower temperatures. Another anisotropy seen in the low-temperature $M(T,H)$ data is the anisotropic field dependence of T_N. T_N is found to be approximately field independent ($T_N\approx6$ K) for $\mathbf{H}\|\mathbf{c}$, but for $\mathbf{H}\perp\mathbf{c}$ T_N is suppressed as H^2 from $T_N\cong6$ K for $H=0$ to below 2 K for $H=20$ kG.

Electrical resistivity ρ_{ab} measurements have been carried out for 2 K $<T<400$ K for current flowing in the ab plane. The high-temperature resistivity shows a negative curvature for $T>150$ K. Since the ρ_{ab} value at 400 K indicates a very short mean free path of ~1.7 Å, the negative curvature in $\rho_{ab}(T)$ suggests saturation as previously observed in, e.g., A-15 compounds. The low-temperature magnetoresistivity data yielded the detailed field dependences of T_N and T_c. These $T_N(H)$ data agree well with the field-dependent T_N data determined from the $M(T,H)$ data described above. The $H_{c2}(T)$ data show anisotropy not only in magnitude but also in temperature dependence, H_{c2} for $\mathbf{H}\|\mathbf{c}$ is larger than H_{c2} for $\mathbf{H}\perp\mathbf{c}$ at all temperatures. This is consistent with the normal state $M(T,\mathbf{H}\perp\mathbf{c})>M(T,\mathbf{H}\|\mathbf{c})$ observed in this temperature range. Perhaps of greater interest is the anisotropic temperature dependence of H_{c2}. For $\mathbf{H}\|\mathbf{c}$ there is a well-defined cusp in H_{c2} at $T_N=6$ K, while for $\mathbf{H}\perp\mathbf{c}$ there is only a broad plateaulike feature between 5 and 6 K. This anisotropy in the temperature dependence of H_{c2} is thought to arise from the anisotropic field dependence of T_N. Evidently, for $\mathbf{H}\|\mathbf{c}$ the relative field independence of T_N leads to a well-defined cusp in H_{c2} associated with the AF ordering, while for $\mathbf{H}\perp\mathbf{c}$ the field dependence of T_N leads to a broad feature in H_{c2} near $T_N(H)$. The $H_{c2}(T)$ for $\mathbf{H}\|\mathbf{c}$, with the cusp, is strikingly similar to $H_{c2}(T)$ calculated for the antiferromagnetic superconductor RMo_6S_6.[32] Given the availability of high-quality single crystals and the easily accessible superconducting and magnetic phase transition temperatures, $ErNi_2B_2C$ should be of great use to test future theoretical predictions of the interplay between superconductivity and local moment magnetism.

ACKNOWLEDGMENTS

Ames Laboratory is operated for the U.S. Department of Energy by Iowa State University under Contract No. W-7405-Eng-82. The work at Ames was supported by the Director for Energy Research, Office of Basic Energy Sciences.

[1]Ø. Fischer, M. Decroux, A. Treyvaud, R. Chevrel, and M. Sergent, Solid State Commun. **17**, 721 (1975).

[2]R. N. Shelton, R. W. McCallum, and H. Adrian, Phys. Lett. **56A**, 213 (1976).

[3]B. T. Matthias, E. Corenzwit, J. M. Vandenberg, and H. E. Barz, Proc. Nat. Acad. Sci. USA **74**, 1334 (1977).

[4]R. Nagarajan, Chandan Mazumdar, Zakir Hossain, S. K. Dhar, K. V. Gopalakrishnan, L. C. Gupta, C. Godart, B. D. Padalia, and R. Vijayaraghavan, Phys. Rev. Lett. **72**, 274 (1994).

[5]R. J. Cava, H. Takagi, H. W. Zandbergen, J. J. Krajewski, W. F. Peck, Jr., T. Siegrist, B. Batlogg, R. B. van Dover, R. J. Felder, K. Mizuhashi, J. O. Lee, H. Eisaki, and S. Uchida, Nature (London) **367**, 252 (1994).

[6]T. Siegrist, H. W. Zandbergen, R. J. Cava, J. J. Krajewski, and W. F. Peck, Jr., Nature (London) **367**, 254 (1994).

[7]Warren E. Pickett and David J. Singh, Phys. Rev. Lett. **23**, 3702 (1994); L. F. Mattheiss, Phys. Rev. B **49**, 13 279 (1994).

[8]P. C. Canfield, B. K. Cho, D. C. Johnston, D. K. Finnemore, and M. F. Hundley, Physica C **230**, 397 (1994); P. C. Canfield, B. K. Cho, D. C. Johnston, and M. F. Hundley (unpublished).

[9]M. Xu, P. C. Canfield, J. E. Ostenson, D. K. Finnemore, B. K. Cho, Z. R. Wang, and D. C. Johnston, Physica C **227**, 321 (1994); M. Xu, B. K. Cho, P. C. Canfield, D. K. Finnemore, D. C. Johnston, and D. E. Farrell, *ibid.* **235-240**, 2533 (1995).

[10]B. K. Cho, Ming Xu, P. C. Canfield, L. L. Miller, and D. C. Johnston, preceding paper, Phys. Rev. B **52**, 3676 (1995).

[11]P. Dervenagas, J. Zarestky, C. Stassis, A. I. Goldman, P. C. Canfield, and B. K. Cho, Physica B (to be published).

[12]A. I. Goldman, C. Stassis, P. C. Canfield, J. Zarestky, P. Dervenagas, B. K. Cho, D. C. Johnston, and B. Sternlieb, Phys. Rev. B **50**, 9668 (1994).

[13]T. E. Grigereit, J. W. Lynn, Q. Huang, A. Santoro, R. J. Cava, J. J. Krajewski, and W. F. Peck, Jr., Phys. Rev. Lett. **73**, 2756 (1994).

[14]J. Zarestky, C. Stassis, A. I. Goldman, P. C. Canfield, P. Dervenagas, B. K. Cho, and D. C. Johnston, Phys. Rev. B **51**, 678 (1995).

[15]S. K. Sinha, J. W. Lynn, T. E. Grigereit, Z. Hossain, L. C. Gupta, and R. Nagarajan, Phys. Rev. B **51**, 681 (1995).

[16]H. Eisaki, H. Takagi, R. J. Cava, K. Mizuhashi, J. O. Lee, B. Batlogg, J. J. Krajewski, W. F. Peck, Jr., and S. Uchida, Phys. Rev. B **50**, 647 (1994).

[17]R. Bachman, F. J. Disalvo, Jr., T. H. Geballe, R. L. Green, R. E. Howard, C. N. King, H. C. Kirsch, K. N. Lee, R. E. Schwall, H. U. Thomas, and R. B. Zubeck, Rev. Sci. Instrum. **43**, 205 (1972).

[18]C. Stassis, A. I. Goldman, P. Dervenagas, J. Zarestky, P. C. Canfield, B. K. Cho, D. C. Johnston, and B. Sternlieb (unpublished).

[19]John L. Prather, U. S. National Bureau of Standards, Monograph No. 19 (1961).

[20]Pierre Boutron, Phys. Rev. B **7**, 3226 (1973).
[21]Roger W. Cohen, G. D. Cody, and John J. Halloran, Phys. Rev. Lett. **9**, 840 (1967).
[22]J. S. Kim, W. W. Kim, and G. R. Stewart, Phys. Rev. B **50**, 3485 (1994); S. A. Carter, B. Batlogg, R. J. Cava, J. J. Krajewski, W. F. Peck, Jr., and H. Takagi, *ibid.* **50**, 4216 (1994).
[23]R. Movshovich, M. F. Hundley, J. D. Thompson, P. C. Canfield, B. K. Cho, and A. V. Chubukov, Physica C **227**, 381 (1994).
[24]M. E. Fisher, Philos. Mag. **7**, 1731 (1962).
[25]M. T. Hutchings, in *Solid State Physics: Advances in Research and Application,* edited by Frederick Seitz and David Turnbull (Academic, New York, 1964), Vol. 16, p. 227, and references therein.
[26]B. K .Cho, B. N. Harmon, D. C. Johnston, and P. C. Canfield (unpublished).
[27]J. E. Greedan and V. U. S. Rao, J. Solid State Chem. **6**, 387 (1973).
[28]B. D. Dunlap, L. N. Hall, F. Behroozi, G. W. Crabtree, and D. G. Niarchos, Phys. Rev. B **29**, 6244 (1984).
[29]V. Ivanov, L. Vinokurova, A. Szytula, and A. Zygmunt, J. Alloys Comp. **191**, 159 (1993).
[30]For a reivew, see Ø. Fischer, in *Ferromagnetic Materials,* edited by K. H. J. Buschow and E. P. Wohlfarth (North-Holland, Amsterdam, 1990), Vol. 5, p. 465.
[31]T. V. Ramakrishnan and C. M. Varma, Phys. Rev. B **24**, 137 (1981).
[32]Kazushige Machida, Kazuo Nokura, and Takeo Matsubara, Phys. Rev. B **22**, 2307 (1980).
[33]N. R. Werthamer, E. Helfand, and P. C. Hohenberg, Phys. Rev. **147**, 295 (1966).